Acoustical imaging with bending waves based on sparse inversion

Lars Hörchens and Diemer De Vries

University of Technology Delft, Lorentzweg 1, 2628 CJ Delft, Netherlands
l.horchens@tudelft.nl

Bending waves can be employed in the context of acoustical imaging for the detection of material defects or localization of vibration sources. The obtainable spatial resolution is limited by the minimal wavelength contained in the excitation signal. The evanescent part of the wave field can usually not be used for the imaging of sources at distances exceeding a wavelength. Therefore only the propagating part of the field can be employed, which means that the minimum size of the region where energy can be focused is in the order of half a wavelength due to the diffraction limit. If the recovery of vibration sources and reflections is posed as an inverse problem, regularization techniques can be applied in order to force a sparse solution. Preliminary results indicate that the assumption of a sparse source distribution can be used to resolve features significantly smaller than half a wavelength. The approach is therefore applied as a high-resolution imaging technique for bending wave fields.

1 Introduction

Acoustical imaging based on bending waves can be employed for source characterization and detection of inhomogeneities in plate-like structures. In acoustical imaging, measurements of the vibration response at a number of positions are employed to create a spatial map indicating the position and strength of these inhomogeneities diffracting the incident field.

If the distance between the diffracting points and the receivers exceeds a wavelength, the evanescent part of the wave field can usually not be employed for imaging. Therefore, only the propagating part of the field can be used; the obtainable spatial resolution is then in the order of half a wavelength.

In the work presented in this paper, a least-squares inversion approach is used to obtain an estimated acoustical image from measurements taken on a line array.

Sacchi et al. have shown in the context of Fourier [1] and Radon transforms [2] that imposing the assumption of sparseness on an inversion scheme can help to increase the obtained resolution. Their approach is transferred and adapted to the imaging problem.

The forward model is introduced in section 2, followed by the inversion approach in section 3. The proposed method is tested on numerical simulations, which are presented in section 4.

2 Forward modeling

The coordinate system is chosen such that the plate under investigation extends in the $x-y$ plane. A line array of receivers is positioned at $y = 0$. The model domain M to be imaged is situated at $y > 0$; it is insonified by a source at $x = 0$, $y = -y_0$. This setup is shown in Fig. (1).

The incident field $v_{\mathrm{inc}}(t, x, y)$ can be computed at every point in M using the Green's function $G(k, r)$ as given in [3]:

$$G(\omega, r) = H_0^{(2)}(\frac{\omega}{c}r) - H_0^{(2)}(-i\frac{\omega}{c}r). \qquad (1)$$

$H_0^{(2)}$ is the zero-order Hankel function of the second kind, i is the imaginary unit, ω represents the frequency, c the phase velocity and r the distance to the source. The spectrum and position of the source determine the incident field; they are assumed to be known. The incident field can therefore be removed from the measurement before the processing is done.
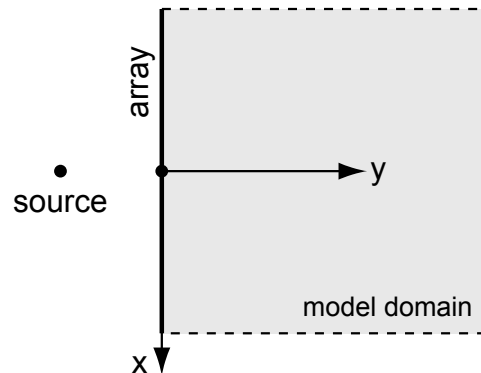

Figure 1: Setup of the model domain.

Scattering objects inside M are represented by the distribution $m(x, y)$. The scattered field $v_{\mathrm{sc}}(t, x, y)$ is modeled using the Born approximation:

$$v_{\mathrm{sc}}(t, x, y) = [v_{\mathrm{inc}}(t, x, y) \cdot m(x, y)] * G(t, x, y), \qquad (2)$$

where $*$ denotes spatio-temporal convolution.

The data domain D is formed by the measured field $d(t, x)$ and is obtained by taking a slice at $y = 0$:

$$d(t, x) = v_{\mathrm{sc}}(t, x, 0). \qquad (3)$$

2.1 Forward operator

The forward model can be described by an operator $\mathcal{L}$ mapping from the model domain M to the data domain D:

$$\mathcal{L} : M \rightarrow D. \qquad (4)$$

For discretized domains, $\mathcal{L}$ could be represented by a matrix. Assuming that M has dimensions $N_x \times N_y$ and D has dimensions $N_t \times N_x$, the size of the matrix required would be $(N_x \cdot N_y) \times (N_t \cdot N_x)$. Such a matrix would be huge, even for small datasets. It is therefore advisable to represent $\mathcal{L}$ by the operations needed for the mapping from M to D.

The spatio-temporal convolution in Eq. (2) can be carried out in the wavenumber-frequency domain. In this domain, the transform variables ω, k_x, k_y correspond to the variables t, x, y in the space-time domain, respectively. Zero-padding is required in order to avoid wraparound effects in the space-time domain.

The operation of taking a slice at $y = 0$ as described in Eq. (3) can also be performed in the wavenumber-frequency domain and is equivalent to the calculation of the average value along the k_y-axis.

Summarizing all operations, the forward mapping consists of the following steps:

1. multiplication of the incident field $v_{inc}(t, x, y)$ by the scattering distribution $m(x, y)$

2. zero-padding in three dimensions (t, x, y)

3. forward Fourier transform in three dimensions $(t, x, y \rightarrow \omega, k_x, k_y)$

4. multiplication by the Green's function $G(\omega, k_x, k_y)$

5. averaging along the k_y axis

6. inverse Fourier transform in two dimensions $(\omega, k_x \rightarrow t, x)$

7. truncation in two dimensions (t, x).

The steps forming the forward operator $\mathcal{L}$ are mathematically represented by Eq. (5) at the bottom of this page. The padding and truncation operations have been left out to simplify the notation.

3 Inversion approach

The forward operation is given by the application of the operator to the model domain:

$$\mathcal{L}m(x, y) = d(t, x). \tag{6}$$

Given the data, an estimate of the model space can be obtained by least-squares inversion. Eq. (7) shows the normal equations for the given problem:

$$\mathcal{L}^*\mathcal{L}m(x, y) = \mathcal{L}^*d(t, x). \tag{7}$$

3.1 Adjoint operator

In order to solve the problem, the adjoint operator $\mathcal{L}^*$ is derived using the inner product [4]:

$$\langle \mathcal{L}m(x, y), d(t, x) \rangle = \langle m(x, y), \mathcal{L}^*d(t, x) \rangle. \tag{8}$$

The adjoint operator $\mathcal{L}^*$ derived using Eq. (8) is given by Eq. (9) at the bottom of this page.

3.2 Smooth inversion

A standard inversion approach using Tikhonov regularization is shown in Eq. (10):

$$\hat{m}(x, y) = \left(\mathcal{L}^*\mathcal{L} + \lambda I\right)^{-1} \mathcal{L}^*d(t, x). \tag{10}$$

In this equation, I represents a variable having the dimension of the model domain $(N_x \times N_y)$ filled with ones,

and λ is a regularization parameter. The application of this kind of regularization is equivalent to assuming a Gaussian distribution of the values of the model domain $\hat{m}(x, y)$ to be estimated [2], thereby imposing smoothness on the result.

3.3 Sparse inversion

As an alternative approach, the model parameters can be assumed to obey a Cauchy distribution, thereby favoring sparsely distributed scatterers. If this assumption is justified, the obtainable resolution of the estimated result can be increased.

The regularized estimation employing a sparseness constrained is given by Eq. (11), which is derived analogously to [1]:

$$\hat{m}(x, y) = \left(\mathcal{L}^*\mathcal{L} + \lambda Q(x, y)\right)^{-1} \mathcal{L}^*d(t, x). \tag{11}$$

The regularization variable $Q(x, y)$ depends on the result of the estimation:

$$Q(x, y) = \frac{1}{1 + \frac{\hat{m}(x,y)\hat{m}^*(x,y)}{2\sigma_m^2}}. \tag{12}$$

Therefore, Eq. (11) is nonlinear and has to be solved iteratively. In each iteration, $Q(x, y)$ is updated from the estimation result $\hat{m}(x, y)$ of the last iteration.

The variable $Q(x, y)$ can be interpreted as a spatially dependent regularization operator, smoothing the result only in regions in which the amplitude of the estimated model space is low. The parameters λ and σ_m have to be chosen depending on the desired sparseness level and the strength of the noise present in the dataset.

4 Simulations

4.1 Setup

Numerical simulations have been carried out for three different configurations of diffracting objects in an aluminum plate having a thickness of 1 mm. The different least-squares problems are solved using a conjugate gradient scheme which is applied to the normal equations [5].

The source inducing the vibrations was positioned at $(x = 0\,\text{cm}, y = -5\,\text{cm})$. A zero-phase signal was emitted with a spectrum having a central frequency of 3 kHz and exhibiting a cosine-squared roll-off towards 0 kHz and 6 kHz. Fig. 2 shows the wavelength in the chosen material for the frequency range of interest.

$$\mathcal{L}m(x, y) = \frac{1}{N_t N_x} \sum_{\omega=0}^{N_t-1} \sum_{k_x=0}^{N_x-1} e^{2\pi i \left(\frac{\omega t}{N_t} + \frac{k_x x}{N_x}\right)} \frac{1}{N_y} \sum_{k_y=0}^{N_y-1} G(\omega, k_x, k_y) \sum_{t=0}^{N_t-1} \sum_{x=0}^{N_x-1} \sum_{y=0}^{N_y-1} e^{-2\pi i \left(\frac{\omega t}{N_t} + \frac{k_x x}{N_x} + \frac{k_y y}{N_y}\right)} v_{inc}(t, x, y) m(x, y) \tag{5}$$

$$\mathcal{L}^*d(t, x) = \sum_{t=0}^{N_t-1} v_{inc}^*(t, x, y) \frac{1}{N_t N_x N_y} \sum_{\omega=0}^{N_t-1} \sum_{k_x=0}^{N_x-1} \sum_{k_y=0}^{N_y-1} e^{2\pi i \left(\frac{\omega t}{N_t} + \frac{k_x x}{N_x} + \frac{k_y y}{N_y}\right)} G^*(\omega, k_x, k_y) \sum_{t=0}^{N_t-1} \sum_{x=0}^{N_x-1} e^{-2\pi i \left(\frac{\omega t}{N_t} + \frac{k_x x}{N_x}\right)} d(t, x) \tag{9}$$
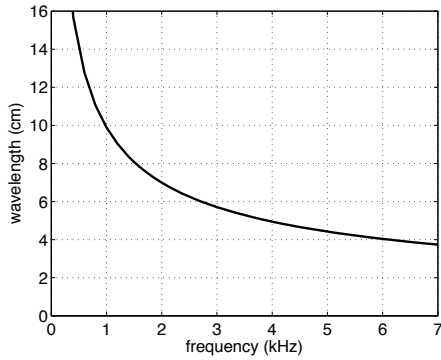
Figure 2: Wavelength in a 1 mm aluminum plate.

4.2 Simulation setup A

A domain of 50 by 50 points with a grid spacing of 1 cm is chosen to be imaged using 50 receivers with a spacing of 1 cm situated at $y = 0$. Fig. 3 shows the first test setup: two diffracting objects are positioned at a distance of 2 cm, the upper one with a relative strength of 0.8, the lower one with a relative strength of 1. Note that the distance of the objects is half a wavelength with respect to the maximum frequency employed in the simulation. For the center frequency, it is only about one third of the wavelength.
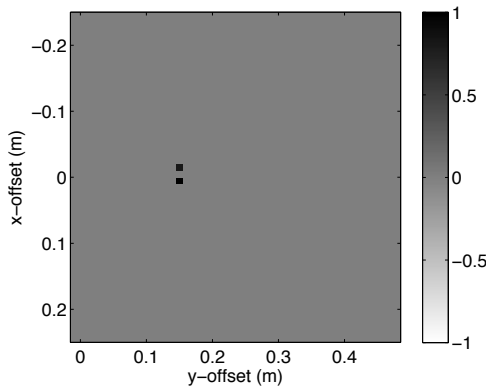
Figure 3: Setup A with two diffracting objects.

The forward simulation $d(t, x) = \mathcal{L}m(x, y)$ is carried out. White noise is added at a level of -20 dB. The result is shown in Fig. 4.
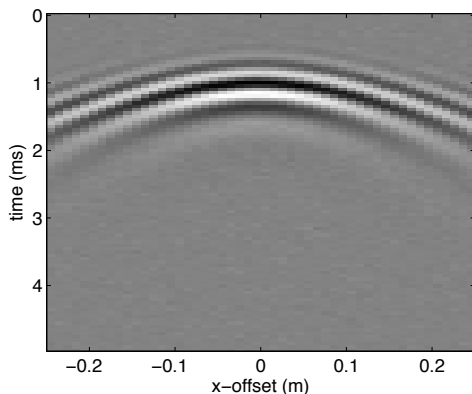
Figure 4: Measured signal $d(t, x)$.

A first estimation of the diffracting structure can be calculated by application of the adjoint operator to the measured dataset. Fig. 5 depicts the reconstruction that can be obtained using $\hat{m}(x, y) = \mathcal{L}^* d(t, x)$.
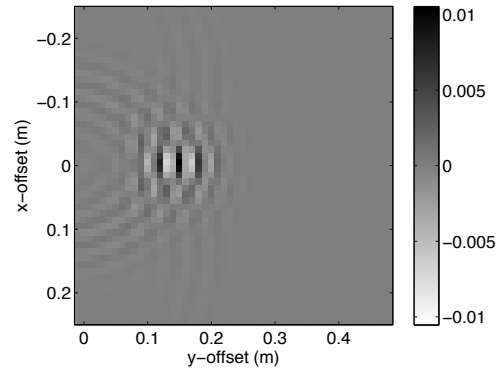
Figure 5: Estimation obtained by application of the adjoint operator $\mathcal{L}^*$.

The resolution can be improved by calculation of the smooth inversion scheme according to Eq. (10) as shown in Fig. 6.
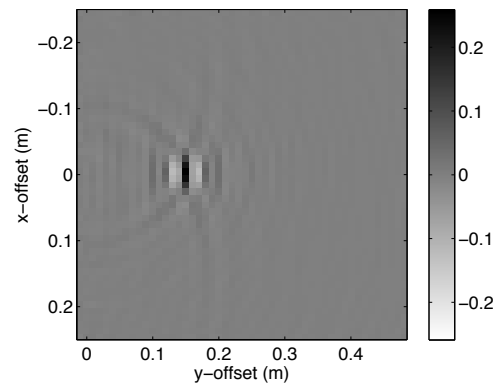

Figure 6: Estimation obtained by application of the smooth inversion operator.

For the sparse inversion according to Eq. (11), an initial guess for the regularization variable $Q(x, y)$ has to be provided. It is chosen to obtain this guess from the result achieved with the adjoint operator presented in Fig. 5.

Fig. 7 depicts the initialization of $Q(x, y)$. It can be seen that $Q(x, y)$ is small in regions where there are higher amplitudes present in the dataset.

The final result of the sparse inversion is shown in Fig. 8. Using the sparseness assumption, the objects having a distance smaller than half a wavelength can be separated. Furthermore, the relative strength is retrieved correctly with values of 0.803 for the upper and 0.994 for the lower scatterer.
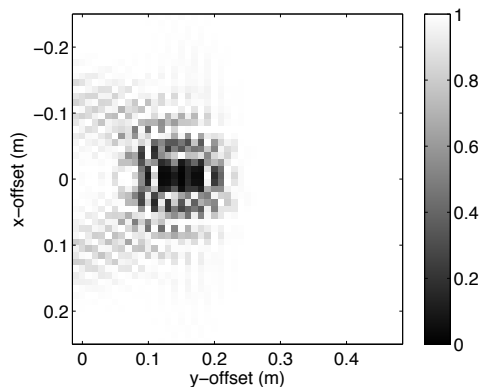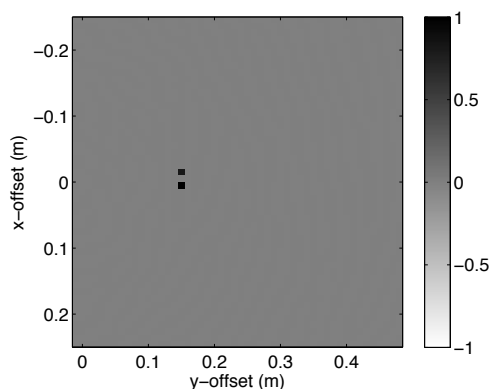
Figure 7: Initial guess of $Q(x, y)$.

Figure 8: Result obtained by sparse inversion

4.3   Simulation setup B

In a second setup, several scatterers of different strength have been positioned inside the model domain as shown in Fig. 9. The estimated distribution of scattering objects obtained by application of the adjoint operator, the smooth inversion scheme and the sparse inversion are shown in Figs. 10, 11 and 12, respectively.
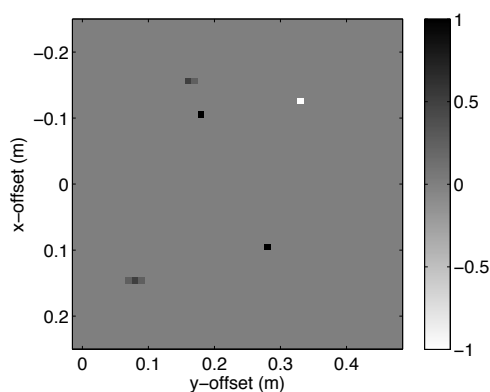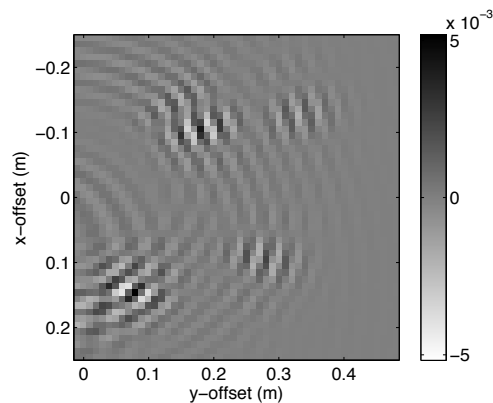

Figure 9: Setup B with several diffracting objects.

The relative performance of the different methods is similar to the results obtained from the first setup. The estimate based on sparse inversion delivers a very satisfactory and useful approximation.
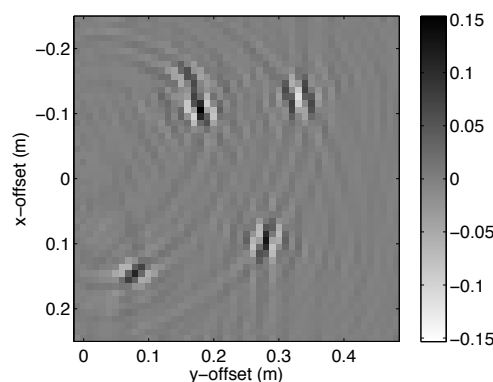

Figure 10: Estimation obtained by application of the adjoint operator $\mathcal{L}^*$.

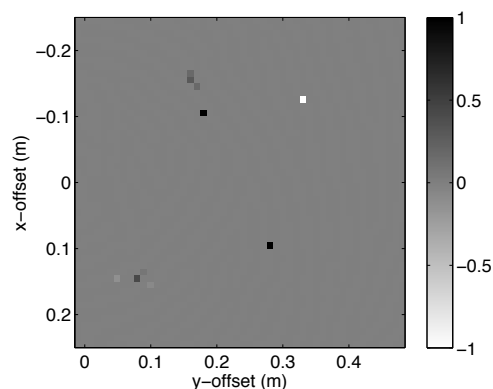Figure 11: Estimation obtained by application of the smooth inversion operator.

Figure 12: Result obtained by sparse inversion

4.4   Simulation setup C

The third simulation features a connected, line-shaped object depicted in Fig. 13. The estimate delivered by the adjoint operator does not provide clear information on the shape of the diffracting structure as can be seen in Fig. 14. Fig. 15 shows the result of the smooth inversion which is good enough to roughly identify orientation and size of the object. Nevertheless, the sparse estimate presented in Fig. 16 is clearly superior in terms of resolution, although it must be stated that the weaker parts of the object can not be found in the reconstruction.
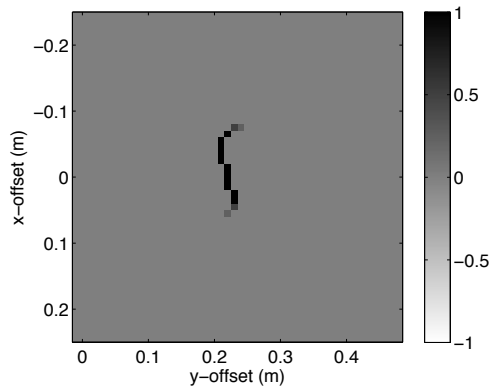
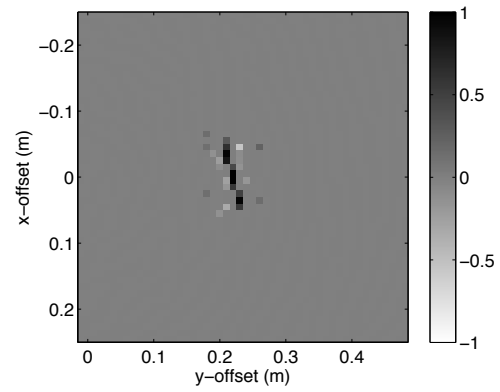Figure 13: Setup C showing a connected object.
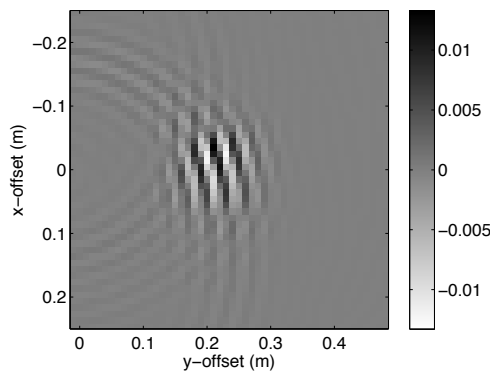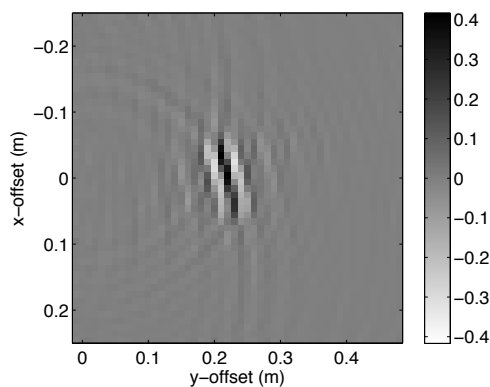

Figure 16: Result obtained by sparse inversion

Figure 14: Estimation obtained by application of the adjoint operator $\mathcal{L}^*$.

Figure 15: Estimation obtained by application of the smooth inversion operator.

5 Conclusion

In this paper, a discrete operator for modeling the measurements on a line array due to a distribution of diffracting objects has been presented. Furthermore, a corresponding adjoint operator has been derived. These operators have been applied in order to obtain estimates of the spatial distribution of scattering objects. Results obtained using three different methods – the adjoint operator, a smooth inversion scheme and a sparse inversion scheme – have been presented and compared for three different simulation examples.

The inversion based on a sparseness assumption obtained superior results and provided estimates with high spatial resolution. In some cases, features smaller than half a wavelength could be resolved. It is however important to keep in mind that meaningful results can only be obtained if the assumption of sparseness is justified for the distribution under investigation.

It is intended to extend the presented work by carrying out experiments in order to test the applicability of the method to real measurements.

Acknowledgments

References

[1] M. Sacchi, T. Ulrych, C. Walker, "Interpolation and Extrapolation Using a High-Resolution Discrete Fourier Transform", *IEEE Transactions on Signal Processing* vol. 46, no. 1, 31-38 (1998)

[2] D. Trad, T. Ulrych, M. Sacchi, "Latest views of the sparse Radon transform", *Geophysics*, vol. 68, no. 1, 386-399 (2003)

[3] L. Cremer, M. Heckl, B. Petersson, "Structure-Borne Sound", 3rd edition, Springer, Berlin (2005)

[4] C. D. Cantrell, "Modern Mathematical Methods for Physicists and Engineers", Cambridge University Press (2000)

[5] J. R. Shewchuk, "An Introduction to the Conjugate Gradient Method without the Agonizing Pain", Technical Report, School of Computer Science, Carnegie Mellon University (1994)